J. Fluid Mech. (2010), *vol.* 658, *pp.* 492–508.
doi:10.1017/S0022112010001813

Viscous selection of an elliptical dipole

ZIV KIZNER[1,2]†, RUVIM KHVOLES[1] AND DAVID A. KESSLER[2]

[1]Department of Mathematics, Bar-Ilan University, Ramat-Gan 52900, Israel
[2]Department of Physics, Bar-Ilan University, Ramat-Gan 52900, Israel

(Received 12 November 2009; revised 11 April 2010; accepted 12 April 2010; first published online 20 July 2010)

A theory of viscous evolution and selection of symmetric two-dimensional dipoles is suggested, based on a combination of numerical simulations and an asymptotic analysis, where the slow time scale associated with the vorticity diffusion due to viscosity is incorporated. It is shown that viscosity first brings a dipole to an intermediate asymptotic state, which is independent of the initial conditions, and then slowly takes the dipole away from this state. We demonstrate that, among the variety of possible ideal-fluid dipole solutions, viscosity going to zero selects a unique solution, which is described to high accuracy by the elliptical dipole solution with a separatrix aspect ratio of 1.037.

Key words: vortex dynamics, vortex flows, vortex interactions

1. Introduction

Mesoscale vortices are present everywhere in the ocean and atmosphere, the most abundant being monopoles and dipoles. During the past three decades, considerable progress has been made in developing the theory of dipole vortices in the context of the Euler equations in two dimensions, and as applied to rotating and stratified fluids in the quasi-geostrophic and shallow-water approximations (see e.g. Kizner & Reznik 2010, and references therein). However, the fundamental groundwork for the construction of dipole solutions was laid out a century ago by Lamb (1895) and Chaplygin (1903), who suggested independently the first regular solution for a two-dimensional ideal-fluid steadily translating symmetric vortical dipole composed of two equal and oppositely signed vortices (see also Meleshko & van Heijst 1994, where these works are discussed).

A two-dimensional Euler flow stationary in some moving frame of reference is characterized by a functional relation between the flow vorticity ζ and the co-moving streamfunction Ψ. In a steadily moving localized vortical structure, the graph of this relation necessarily consists of (at least) two branches, the straight line $\zeta = 0$ for the region outside the vortices, and a generally curved line representing the interior region (in sufficiently complex vortices, the interior ζ versus Ψ relation can split into a number of subbranches; see Kizner, Berson & Khvoles 2003).

Recently, a class of ideal-fluid (inviscid) elliptical dipole solutions was suggested, constructed by a combination of analytical and numerical methods: symmetric dipoles with separatrices extended along the dipole translational axis x (below we term them squeezed dipoles) were suggested by Boyd & Ma (1990), and those with

† Email address for correspondence: zinovyk@mail.biu.ac.il

separatrices extended in the transverse, y direction by Kizner & Khvoles (2004) and Khvoles, Berson & Kizner (2005). To within a similarity transformation, an elliptical dipole is determined by its aspect ratio, $\epsilon = r_y/r_x$, where r_y and r_x are the radii of its separatrix in the y and x directions. At $\epsilon = 1$ (the Lamb–Chaplygin dipole), the interior ζ versus Ψ relation is linear, while at $\epsilon \neq 1$ it is nonlinear, and the stronger the deviation from a circle, the stronger the nonlinearity. The solutions with separatrices extended in the y direction are of special interest since, in laboratory experiments and numerical simulations, the dipoles eventually evolve to quasi-elliptical states with $\epsilon > 1$ (e.g. Khvoles *et al.* 2005; Trieling *et al.* 2010). In fact, ideal-fluid dipoles with separatrices different from ellipses can also be constructed. For example, Cassini ovals and some other symmetric convex contours slightly deviating from ellipses can be taken as separatrices. Thus, there is a continuous family of inviscid steady-state dipole solutions. Importantly, the dipole shape and the form of the ζ versus Ψ relation are in one-to-one correspondence; this idea was proposed by Boyd & Ma (1990) and strengthened by Kizner *et al.* (2003).

In numerical simulations of vortex dynamics, weak viscosity is often introduced to eliminate small-scale enstrophy irregularities. Of course, this destroys the Hamiltonian structure of the dynamical system under consideration. However, the fact that introduction of viscosity might change qualitatively the characteristics of a two-dimensional symmetric dipole was generally unappreciated until recently. In the absence of external forcing, an obvious effect of viscosity is increasing the dipole size and weakening its amplitude and propagation speed with time. Less obvious is the tendency of symmetric dipoles towards a specific shape (discussed below).

The questions that immediately arise are: whether the existence of a continuous family of inviscid dipole shapes is a result of the idealization of the small-viscosity physical flow by the zero-viscosity Euler limit. And if so, whether viscosity represented in the vorticity evolution equation by the term $\nu\Delta\zeta$ (where ν is the kinematic coefficient of viscosity) selects a unique shape from the variety of symmetric ideal-fluid dipole solutions. Or, more precisely, whether with the passage of time a unique limiting shape is achieved by a properly scaled decaying symmetric dipole as viscosity decreases. Viscosity is a singular perturbation in that it involves the highest derivatives in the equation of vorticity evolution and thus can drastically change the nature of the space of solutions. Such behaviour has been seen with other singular perturbations. For example, surface tension in the Saffman–Taylor problem destroys the continuum of solutions of the zero-surface-tension problem selecting a single stable finger (Kessler, Koplik & Levine 1988).

During the past two decades, some effort has been made to understand the behaviour of decaying dipoles in the framework of non-divergent two-dimensional flows. Swaters (1988, 1991) attempted to develop an asymptotic theory describing the Lamb–Chaplygin dipole under Rayleigh damping as a self-similar solution. His simulations were too short, however, to sufficiently test his theory. Nielsen & Juul Rasmussen (1996), Juul Rasmussen *et al.* (1996), van Geffen & van Heijst (1998) and Sipp, Jacquin & Cossi (2000) saw in their simulations of viscous decay of dipoles the beginnings of the development of the self-similar regime and indications of a viscosity-independent profile, but their simulations were also not long enough to achieve the final profile. Most recently, Delbende & Rossi (2009) have obtained in longer-term numerical simulations a vorticity profile to which the Lamb–Chaplygin dipole converges, and derived the leading-order scaling describing this evolution. However, a number of questions remained unanswered and some important issues overlooked.

In this paper, by combining perturbation methods (where ν is regarded as a small parameter) with the results of numerical simulations at different ν and various initial

conditions, we offer a positive and constructive answer to the above questions. Starting variously from the Lamb–Chaplygin dipole, a squeezed elliptic dipole ($\epsilon = 0.85$), the supersmooth extended dipole ($\epsilon = 1.162$), pairs of Rankine and Gaussian vortices and also from some arbitrarily chosen compact antisymmetric vorticity distributions, we demonstrate that the limiting scaling dipole shape does exist, is independent of initial conditions and is basically identical to the elliptical solution at $\epsilon \approx 1.037$. In addition we show that, at finite ν, at long times there is a secular deviation from the ideal-fluid Eulerian dipole shape, which is governed by a scaling law different from that of the dipole itself.

2. Scaling and the self-similarity ansatz

In this section, we make a first (within this study) attempt to develop a scaling theory for the evolution of a symmetric dipole in the presence of viscosity. This first scaling theory will provide some predictions which, in fact, are in agreement with numerical data. However, we shall see in the next section that this theory is incomplete and that a more accurate theory is needed, which will be provided in § 4.

The vorticity ζ and the streamfunction ψ of a non-divergent two-dimensional flow are related via the Poisson equation

$$\zeta = -\Delta_{X,Y}\psi, \tag{2.1}$$

where X and Y are Cartesian coordinates and $\Delta_{X,Y}$ is the Laplacian operator in these coordinates. The viscous evolution of the vorticity field $\zeta(t, X, Y)$ is governed by the equation

$$\frac{\partial \zeta}{\partial t} + J_{X,Y}(\zeta, \psi) = \nu \Delta_{X,Y}\zeta, \tag{2.2}$$

where t is time and $J_{X,Y}$ is the Jacobian operator in X and Y. All variables in (2.1) and (2.2) are non-dimensional, scaled with the initial dipole size L^* (e.g. the square mean radius $\sqrt{S/\pi}$, where S is the area encircled by the separatrix), initial translation speed U^* and the advective time scale $T_A = L^*/U^*$; ν is accordingly the inverse Reynolds number.

We consider dipoles composed of two symmetric oppositely signed vortices (note that (2.1) and (2.2) preserve symmetry of this type) and, assuming the X-axis to be the symmetry and propagation axis, change to a frame of reference attached to the dipole, with the local coordinates being

$$x = X - X_C, \quad y = Y. \tag{2.3}$$

In (2.3), $X_C = X_C(t)$ is the X-coordinate of the dipole centre, defined e.g. as the X-coordinate of the centroid of one of the vortices constituting the dipole. In the new coordinates, (2.1) and (2.2) become

$$\zeta = -\Delta_{x,y}\psi, \tag{2.4a}$$

$$\frac{\partial \zeta}{\partial t} - U\frac{\partial \zeta}{\partial x} + J_{x,y}(\zeta, \psi) = \nu \Delta_{x,y}\zeta, \tag{2.4b}$$

where $J_{x,y}$ and $\Delta_{x,y}$ are the Jacobian and Laplacian in x and y, U is the dipole translation speed, $U = U(t) = \mathrm{d}X_C/\mathrm{d}t$ and ζ and ψ are understood as functions of t, x and y. In terms of the co-moving streamfunction Ψ defined as $\Psi = \psi + Uy$, (2.4) can be rewritten as

$$\zeta = -\Delta_{x,y}\psi, \tag{2.5a}$$

$$\frac{\partial \zeta}{\partial t} + J_{x,y}(\zeta, \Psi) = \nu \Delta_{x,y}\zeta. \tag{2.5b}$$

In the inviscid limit, a steadily translating dipole ($U = \text{const.}$) is described by the equation

$$J_{x,y}(\zeta, \Psi) = 0. \tag{2.6}$$

Our initial ansatz is that there exists a unique shape to which any symmetric dipole affected by viscosity asymptotically evolves. In such a case, the vorticity distributions achieved at large times, when properly normalized, must become alike both within the same simulation (started from a specific initial state) and between simulations initialized differently. This implies that the asymptotic state, if it exists, must be self-similar in the sense that only the space scale L and the amplitude A of the vorticity distribution are time-dependent, so that the following separation of variables is possible:

$$\zeta(t, x, y) = A(t)\omega(\xi, \eta), \quad \Psi(t, x, y) = A(t)L^2(t)\Phi(\xi, \eta), \tag{2.7}$$

where the scaled local coordinates ξ and η are

$$\xi = \frac{x}{L(t)}, \quad \eta = \frac{y}{L(t)}. \tag{2.8}$$

Setting the streamfunction amplitude in (2.7) to be AL^2 is dictated by dimensionality considerations (see also (2.5*a*)). (In the same manner, it can be shown that the streamfunction ψ can be scaled as $\psi = A(t)L^2(t)\phi(\xi, \eta)$ and that $U = vA(t)L(t)$, i.e. $\Phi = v\eta + \phi$, where v is a constant.)

So, according to this hypothesis, in the scaled co-moving coordinates (2.8), the normalized vorticity and streamfunction fields $\omega(\xi, \eta)$ and $\Phi(\xi, \eta)$ should be time-independent. Substitution of (2.7) and (2.8) into (2.5*b*) yields the equation for the evolution of normalized vorticity:

$$\left(\frac{\dot{A}}{A}L^2\right)\omega - (\dot{L}L)\left[\xi\frac{\partial\omega}{\partial\xi} + \eta\frac{\partial\omega}{\partial\eta}\right] + \left(AL^2\right)J_{\xi,\eta}(\omega, \Phi) = \nu\Delta_{\xi,\eta}\omega, \tag{2.9}$$

where $J_{\xi,\eta}$ and $\Delta_{\xi,\eta}$ are the Jacobian and Laplacian in ξ and η, and the dots designate differentiation with respect to t.

Since the right-hand side of (2.9) is time-independent, for the separation of variables (2.7) to hold, the coefficients in the parentheses in the left-hand side of (2.9) must be constant. The condition $AL^2 = \text{const.}$, although formally compatible with the conditions $\dot{A}L^2/A = \text{const.}$ and $\dot{L}L = \text{const.}$, is physically inappropriate since it implies that the streamfunction amplitude and net energy of the dipole vortex do not decay with time. Therefore, the necessary self-similarity conditions are

$$J(\omega, \Phi) = 0, \tag{2.10}$$

which means that Φ and ω are functionally dependent, and

$$L = L(0)\sqrt{1 + \lambda t}, \quad A = A(0)\left(\frac{L}{L(0)}\right)^{\mu} = A(0)\,(1 + \lambda t)^{\mu/2}, \tag{2.11}$$

where λ and μ are some constants, while $L(0)$ and $A(0)$ are the initial values of L and A. In other words, in the asymptotic regime, ω and Φ must represent an ideal-fluid dipole solution, i.e. the vorticity advection and diffusion must proceed independently, L^2 must be a linear function of t, and $\ln[A/A(0)]$ must be proportional to $\ln[L/L(0)]$:

$$\ln\frac{A}{A(0)} = \mu\ln\frac{L}{L(0)}. \tag{2.12}$$

The above-presented ansatz is tested against numerical simulations in the next section.

3. Numerical simulations

In the numerical simulations presented below, (2.1) and (2.2) are solved using a finite-difference code in a rectangular box $[-15 \leqslant X \leqslant 15; -15 \leqslant Y \leqslant 15]$ with periodic boundary conditions in X, and the condition of the vanishing of ψ at $Y = \pm 15$ (for a detailed description, see Kizner, Berson & Khvoles 2002; Khvoles *et al.* 2005). The computation should be stopped when, due to the periodicity conditions, the vorticity trail in the wake of the dipole comes in contact with the dipole's front part; otherwise a cutting filter should be adopted, consisting of a periodic-in-time blotting out of the peripheral vorticity field (Juul Rasmussen *et al.* 1996; Kizner *et al.* 2002). Starting our simulations from different initial conditions and varying the viscosity coefficient, we studied numerically the viscous evolution of symmetric dipoles. A number of simulations with bigger boxes (40×40, 50×50 and 60×40) did not exhibit any visible changes in the results.

The computations were run at $\nu = 0.02$, 0.002, 0.0002 at a grid spacing of 0.1 for long-term simulations and 0.05 for short-time simulations, being initialized with the following explicit inviscid solutions: a squeezed elliptical dipole with $\epsilon = 0.85$; the Lamb–Chaplygin dipole ($\epsilon = 1$); the supersmooth elliptical dipole with $\epsilon \approx 1.162$; and a moderately extended elliptical dipole with $\epsilon = 1.037$ (at a later stage). All these dipoles had the same translation speed $U = 1$ and initial mean radius $\bar{r} = 1$ (so that the same number of nodes, 11 or 21, fell on the dipole mean radius at $t = 0$). Additional simulations at $\nu = 0.002$ were initialized with dipoles that are not steady-state solutions of ideal Euler flow, namely with pairs of Rankine and Gaussian vortices. Also, a number of simulations were performed initialized with a set of arbitrarily chosen sufficiently compact antisymmetric vorticity distributions. These additional simulations reproduced the same general features as the previously listed runs, in particular, generating at long time the asymptotic dipole discussed below. Therefore, in the interests of brevity, we pass over them in the subsequent presentation.

The fields and parameters tracked in the computations were: the streamfunction and vorticity fields; the coordinates of the centroid of the positive vortex computed as $X_C = \iint X\zeta \, \mathrm{d}X \, \mathrm{d}Y/\Gamma$ and $Y_C = \iint Y\zeta \, \mathrm{d}X \, \mathrm{d}Y/\Gamma$, where the net circulation of the vortex is $\Gamma = \iint \zeta \, \mathrm{d}X \, \mathrm{d}Y$; the second moments of the vorticity distribution in the positive vortex computed as $a_x^2 = \iint (x - X_C)^2 \zeta \, \mathrm{d}x \, \mathrm{d}y/\Gamma$ and $a_y^2 = \iint (y - Y_C)^2 \zeta \, \mathrm{d}x \, \mathrm{d}y/\Gamma$; the dipole translation speed U needed for the calculation of Ψ (estimation of U by differentiation of X_C and by minimization of the Jacobian $J(\zeta, \Psi)$ as a function of U led to essentially the same results); the local maxima ζ_M and Ψ_M of ζ and Ψ within the separatrix; the relative measure $\langle J \rangle$ of the error in (2.6),

$$\langle J \rangle = \sqrt{2 \iint [J(\zeta, \Psi)]^2 \, \mathrm{d}x \, \mathrm{d}y \Big/ \iint \left[\left(\frac{\partial \zeta}{\partial x} \frac{\partial \Psi}{\partial y} \right)^2 + \left(\frac{\partial \Psi}{\partial x} \frac{\partial \zeta}{\partial y} \right)^2 \right] \mathrm{d}x \, \mathrm{d}y}. \tag{3.1}$$

To enable the comparison of the ζ and Ψ fields within the same simulation, we took $L = Y_C$ and $A = \zeta_M$, and scaled the vorticity field with A and the streamfunction with AL^2, and also scaled the co-moving coordinates according to (2.8). The resulting normalized fields are designated as ω and Φ, their maxima (within the separatrix) being 1 and $\Phi_M = \zeta_M / AL^2$, respectively. In the case of $\nu = 0.002$, to test the fulfilment of (2.11) and (2.12), the values of A and L at $t = 500$ (when all the dipoles looked alike) were taken in place of $A(0)$ and $L(0)$. In order to compare the simulations with different ν, it is helpful, in addition to the true time t (which is, in fact, the advective time), to use the viscous time $\tau = \nu t$.

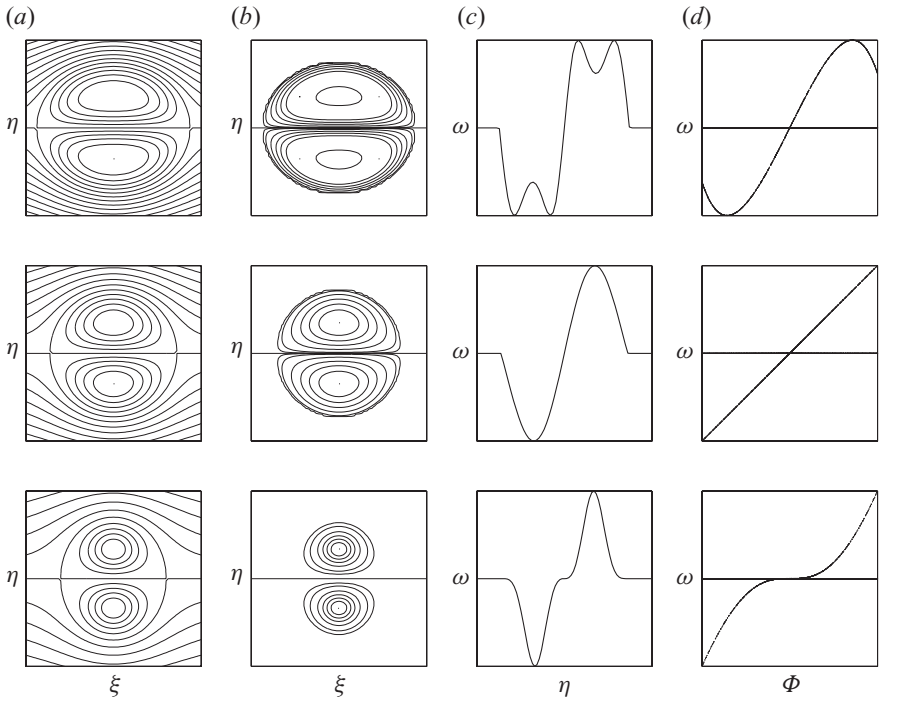

FIGURE 1. The initial dipole states, whose evolution is shown in figures 2, 3, 5 and 7(*c*). (*a*) Scaled co-moving streamfunction fields (contours are given at a 20 % step of the peak value); (*b*) scaled vorticity fields (contours are given at steps of 1 %, 5 %, 20 %, 40 %, 60 % and 80 % of the maximum); (*c*) cross-sections of the scaled vorticity fields passing through the two points of local maximum and minimum; (*d*) graphs of the normalized vorticity ω versus co-moving streamfunction Φ relation (the horizontal line represents the Φ versus ω relation outside the dipole, where the flow is irrotational). From top to bottom: $\epsilon = 0.85$ (squeezed dipole), $\epsilon = 1$ (Lamb–Chaplygin dipole); $\epsilon = 1.162$ (supersmooth dipole). Only the central portion of the fields and profiles is shown: the box dimensions in (*a*) and (*b*) are $-3 \leqslant \xi \leqslant 3$ and $-3 \leqslant \eta \leqslant 3$ (corresponding to $6Y_C \times 6Y_C$ in non-scaled variables), respectively; in (*c*), $-3 \leqslant \eta \leqslant 3$ and $-1 \leqslant \omega \leqslant 1$; in (*d*), $-\Phi_M \leqslant \Phi \leqslant \Phi_M$ and $-1 \leqslant \omega \leqslant 1$.

As is evident from our simulations, at a given ν, after some time, the dipole does not remember the initial state (figures 1 and 2). In accordance with (2.11), the apparent stabilization of the three dipoles in the same normalized state is evidenced by figure 3, where Y_C/a_y saturates with time, and the graphs of $[Y_C/Y_C(0)]^2$ and $[a_y/a_y(0)]^2$ approach straight-line asymptotes that have almost the same slopes $\lambda \approx 0.90$. Also the straight-line asymptotes, to which the graphs of $\ln[A/A(0)]$ versus $\ln[L/L(0)]$ approach, have practically equal slopes, $\mu \approx -3.17$ (see (2.12)).

At a given ν, the scatter-plots of normalized ζ versus normalized Ψ achieved at sufficiently large times (figure 2*d*) look quite similar to each other. Unlike the scatter-plot for the Lamb–Chaplygin dipole, they are somewhat curved, but less curved than that of the supersmooth dipole (cf. figures 1*d* and 2*d*). Therefore, one might guess that the shape assumed by viscously evolving dipoles is, roughly speaking, intermediate between the Lamb–Chaplygin and supersmooth dipoles. Although this is what in fact happens (see § 5), a close inspection of the scatter-plots reveals two facts which indicate that the stabilization in the asymptotic regime cannot be complete.

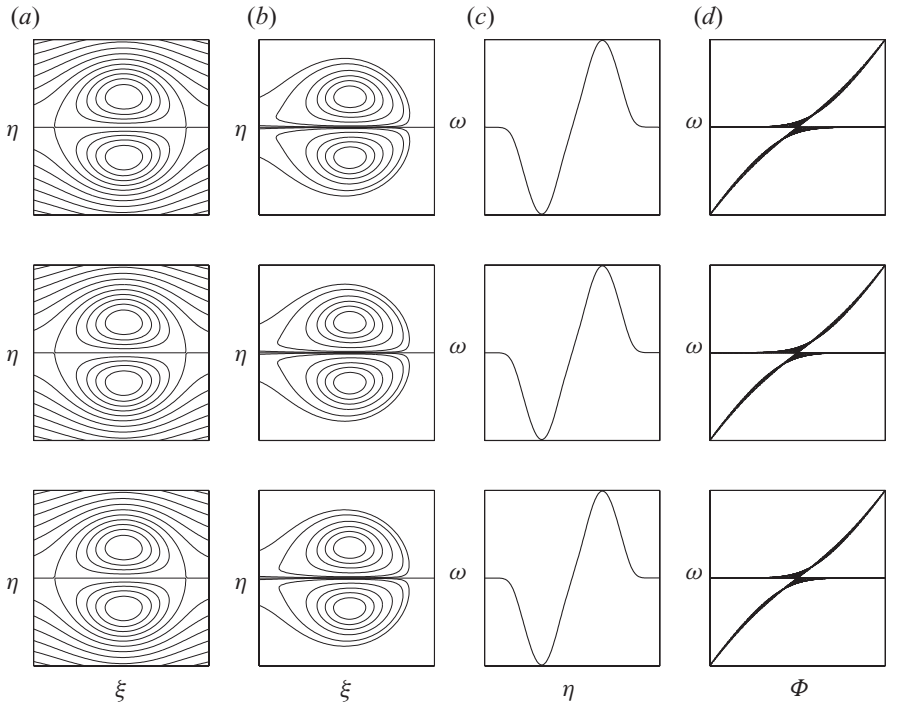

FIGURE 2. The dipole states achieved at $t = 1000$ (i.e. $\tau = 2$) in the simulations with $\nu = 0.002$ initialized with the dipoles shown in figure 1. From top to bottom: the squeezed ($\epsilon = 0.85$), Lamb–Chaplygin ($\epsilon = 1$) and supersmooth ($\epsilon = 1.162$) dipoles. Notations and box sizes as in figure 1.

The first observation is that, although the point scatter in the scatter-plots decreases with decreasing ν, it does not exhibit a long-term tendency to decrease at a fixed ν (figure 4). One of the explanations of this fact is the following. Suppose that the scatter dies away as $t \to \infty$, so that, in this limit, (2.10) is fulfilled exactly and some functional dependence $\omega = F(\Phi)$ exists. Then the vorticity and streamfunction must vanish at the same contours (because they both vanish at the x-axis). In other words, the dipole border and the streamfunction separatrix contour must coincide. In addition to the increase of the dipole's size and weakening of its amplitude, the effect of vorticity diffusion is apparent in the smoothing out of the vorticity profile at the dipole border, that is, in suppressing the derivative of ω normal to this contour (see e.g. vorticity cross-sections in figure 2c). For instance, at the point where the η-axis crosses the separatrix, $\partial\omega/\partial\eta = 0$. Because at this point $\partial\Phi/\partial\eta \neq 0$ and $\Phi = 0$, the equality $\partial\omega/\partial\eta = F'(0)\partial\Phi/\partial\eta = 0$ holds if and only if $F'(0) = 0$ (here F' is the derivative of F). However, on the ξ-axis, where the patches of positive and negative vorticity are immediately neighbouring, the vorticity diffusion causes the existence of a non-zero gradient of ω, and, in terms of normalized variables, this gradient cannot vanish as $t \to \infty$ (figure 2c). Therefore, on the ξ-axis, $\partial\omega/\partial\eta = F'(0)\partial\Phi/\partial\eta \neq 0$, yielding $F'(0) \neq 0$, which is in contradiction with the above-established equality $F'(0) = 0$. This reasoning leads to a general conclusion that, even in the limit of $t \to \infty$, a viscosity-affected dipole (at finite ν) will never reach a self-similar asymptotic regime. Therefore, we term the regime achieved in the simulations a quasi-asymptotic state (or, in other words, an intermediate asymptotics).

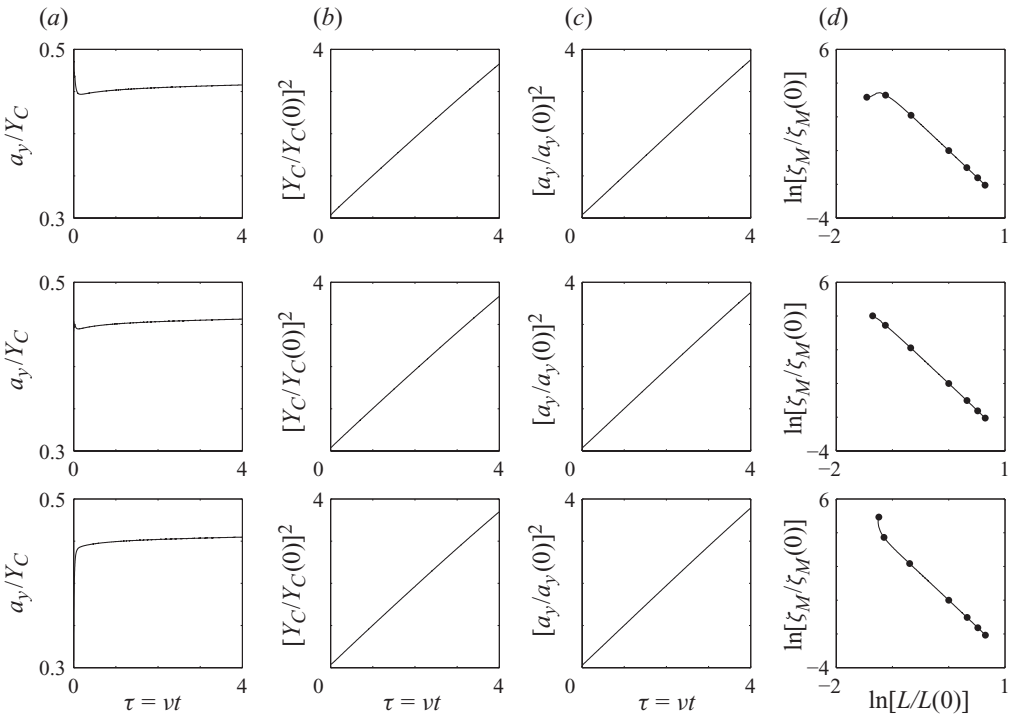

FIGURE 3. Evolution of the dipole parameters in the simulations at $\nu = 0.002$. From top to bottom: the squeezed ($\epsilon = 0.85$), Lamb–Chaplygin ($\epsilon = 1$) and supersmooth ($\epsilon = 1.162$) dipoles. Solid circles in (*d*) indicate the states at $\tau = 0$, 0.04, 0.2, 1, 2, 3 and 4 (i.e. at $t = 0$, 20, 100, 500, 1000, 1500 and 2000).

The second observation is that the relative error in (2.10) not only does not decrease, but it slowly grows with time. This is evidenced both by gradual thickening of the scatter-plots with increasing time at a chosen ν (figure 4) and by the behaviour of $\langle J \rangle$ (figure 5). The latter deserves special consideration.

In discussing the evolution of $\langle J \rangle$ we will confine ourselves to the case of $\nu = 0.002$. The reasons for such a choice are the following. Bearing in mind the question of viscous selection of an inviscid dipole solution, we are most interested in simulations with as small ν as possible. Clearly, to be able to scrutinize the viscous effects, when decreasing ν one has to increase the time period for which the computations are run. On the other hand, when ν is really small (say, $\nu = 0.0002$), an accordingly high space and time resolution must be taken, because otherwise fine viscosity effects can be hidden by the discretization errors; this requirement can unduly increase the duration of computations. A comparison of the results obtained at $\nu = 0.02$, 0.002 and 0.0002 leads us to the conclusion that a good compromise between the above-listed competing factors is to choose $\nu = 0.002$, for which computations can be run both for sufficiently long times and at satisfactory resolution.

At $\nu = 0.002$, three phases in the behaviour of $\langle J \rangle$ can be recognized (figure 5*a*, *b*). Note that any exact dipole solution will satisfy the finite-difference counterpart of (2.6) at a certain error (which can be of significance at a low space resolution). Therefore the first, unavoidable, phase is that of the adjustment of an almost exact ideal-fluid solution (set as the initial condition) to the given space grid. This process (accompanied by the action of viscosity) takes longer in dipoles with a considerable

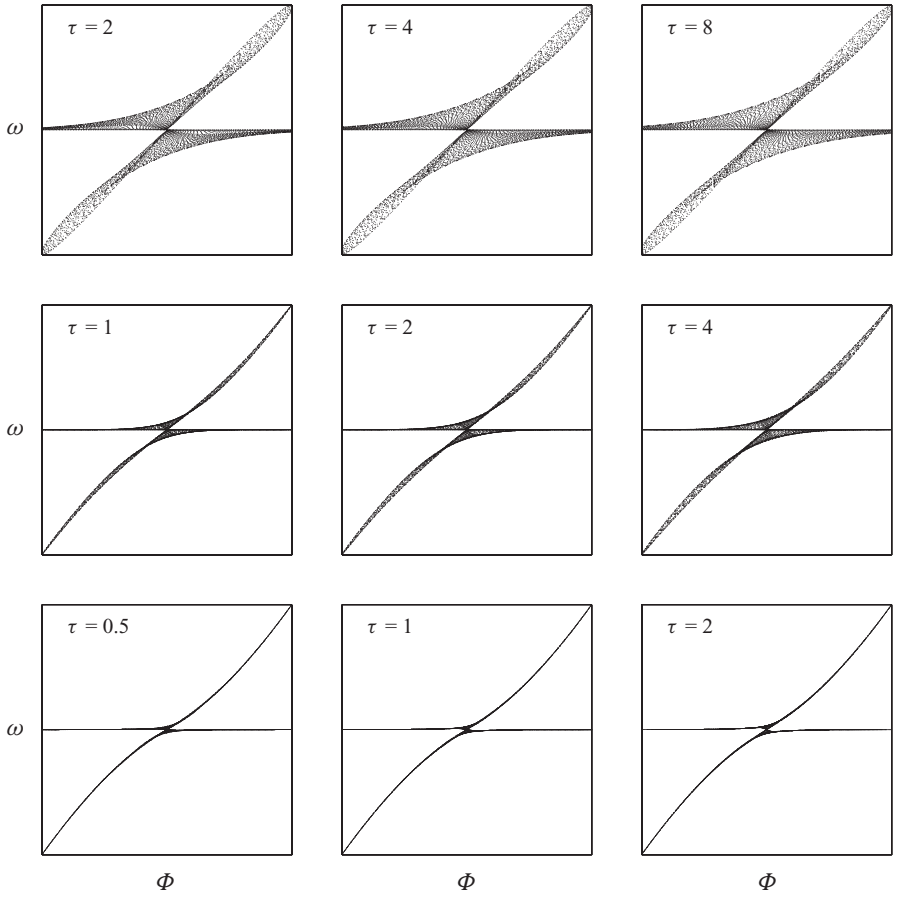

FIGURE 4. Scaled vorticity versus streamfunction scatter-plots achieved at specific time moments in the simulations initialized with the Lamb–Chaplygin dipole at $\nu = 0.02$, $\nu = 0.002$ and $\nu = 0.0002$ (from top to bottom).

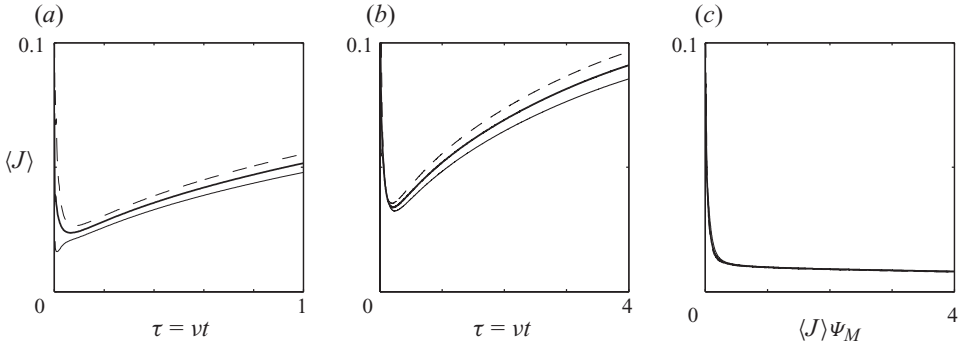

FIGURE 5. Evolution of the deviation from the ideality condition (2.6) in the simulations at $\nu = 0.002$ shown in figures 2 and 3. (*a*) $\langle J \rangle$ against $\tau = \nu t$ in the high-resolution simulations; (*b*) same as in (*a*), but in the low-resolution simulations; (*c*) $\langle J \rangle \Psi_M$ against τ. Broken line, simulation initialized with the squeezed dipole; bold solid line, the Lamb–Chaplygin dipole; thin solid line, the supersmooth dipole.

discontinuity of the vorticity gradient at the separatrix ($\epsilon = 0.85$ and 1) and less in the supersmooth dipole case, lasting for approximately 10–30 advective time units in the high-resolution experiments and approximately 100–120 time units in the low-resolution simulations. In the end of this phase, $\langle J \rangle$ reaches its local minimum (of course, the local minima are smaller in the high-resolution simulations). Next, affected mostly by viscosity, the dipole undergoes some reorganization and achieves the quasi-asymptotic state, which is close to self-similarity. In the third phase, the changes in the dipole structure are hardly visible, but a slow monotonic growth of $\langle J \rangle$ is observed, representing the increasing effect of finite viscosity that slowly takes the dipole away from this state. Noticeably, the results obtained in the simulations at $\nu = 0.002$ with grid spacings of 0.05 and 0.1 are basically the same not only qualitatively, but (from approximately $t = 300$) also quantitatively. For example, in the simulation initialized with the Lamb–Chaplygin dipole, the values of $\langle J \rangle$ reached at $t = 500$ for high and low resolutions are practically identical, $\langle J \rangle \approx 0.0515$. This is not surprising: the increase in the dipole size, caused by viscosity, effectively increases the resolution of the computations, making it sufficient even at the grid spacing of 0.1. Therefore, to study the adjustment of the dipole to the quasi-asymptotic state, running high-resolution simulations for times longer than a few hundred advective time periods is not necessary. In fact, the two kinds of simulations complement each other, one representing correctly the fine effects at relatively short times, and the other, the long-term evolution.

Summarizing our observations, the following interim conclusions can be drawn: (i) at the same ν, different dipoles demonstrate a tendency to evolve towards the same quasi-asymptotic state; (ii) the smaller the ν, the closer the quasi-asymptotic state is to an ideal-flow solution, but at a fixed finite ν, (2.1) will never be fulfilled exactly even in the idealistic limit of $t \to \infty$ and the grid step going to zero; (iii) whatever ν, with the passage of time the viscosity effect increases, the increase becoming evident in the growth of $\langle J \rangle$; (iv) the ansatz of the existence of an exact self-similar asymptotic dipole at a finite ν should be rejected; (v) a more delicate mathematical analysis is needed to explain the observed effects and, possibly, to answer the question of the existence of a limiting dipole shape at $\nu \to 0$.

4. Slow-time asymptotic analysis and the criteria of the existence of a limiting shape

The above results suggest the use of the analysis based on the expansion of vorticity and co-moving streamfunction in an asymptotic series with respect to ν. We shall see that, for the purpose of our analysis, it is sufficient to keep only the zero- and first-order terms in the expansions. Thus the vorticity and co-moving streamfunction are represented as

$$\zeta = \zeta_0(t, x, y) + \nu\zeta_1(t, x, y) + O(\nu^2), \tag{4.1a}$$

$$\Psi = \Psi_0(t, x, y) + \nu\Psi_1(t, x, y) + O(\nu^2). \tag{4.1b}$$

Substitution of (4.1) in (2.5*a*) yields

$$\zeta_0 = -\Delta_{x,y}\Psi_0, \quad \zeta_1 = -\Delta_{x,y}\Psi_1. \tag{4.2}$$

The new basic hypothesis replacing the ansatz presented in § 2 is the existence of the highest possible degree of self-similarity in the quasi-asymptotic solution, consistent with (4.1). The vorticity diffusion due to viscosity is slow relative to advection.

Therefore, we assume the dipole size L to be a function of the viscous time $\tau = \nu t$ only, change to the scaled local coordinates ξ and η defined as

$$\xi = \frac{x}{L(\tau)}, \quad \eta = \frac{y}{L(\tau)}, \tag{4.3}$$

and assume the following separation of variables to hold:

$$\zeta_0(t, x, y) = A_0(\tau)\omega_0(\xi, \eta), \qquad \zeta_1(t, x, y) = A_1(\tau)\omega_1(\xi, \eta), \tag{4.4a}$$

$$\Psi_0(t, x, y) = A_0(\tau)L^2(\tau)\Phi_0(\xi, \eta), \qquad \Psi_1(t, x, y) = A_1(\tau)L^2(\tau)\Phi_1(\xi, \eta). \tag{4.4b}$$

Again dimensionality considerations dictate the amplitudes of Ψ_0 and Ψ_1 to be A_0L^2 and A_1L^2 (see also (4.2)); so $\omega_0 = -\Delta\Phi_0$ and $\omega_1 = -\Delta\Phi_1$. The scheme outlined above is, in fact, a degenerate version of a multi-scale asymptotic analysis that, in general, involves an infinite sequence of times: t, νt, $\nu^2 t$, ... In our analysis only one viscous slow time $\tau = \nu t$ is kept.

Our next step is the substitution of (4.1), (4.3) and (4.4) in (2.5b). Grouping first the terms that do not bear the factor ν, we obtain the equation for the zero-order vorticity and streamfunction fields:

$$J(\omega_0, \Phi_0) = 0, \tag{4.5}$$

where J is the Jacobian in ξ and η. (Clearly, (4.1b) and (4.4b) imply that $\psi = \psi_0(t, x, y) + \nu\psi_1(t, x, y) + O(\nu^2) = A_0L^2\phi_0(\xi, \nu) + \nu A_1L^2\phi_1(\xi, \eta) + O(\nu^2)$, where $\phi_1 = \Phi_1$ and $\phi_0 = \Phi_0 - v\eta$, so that the translation speed is $U = vA_0(\tau)L(\tau)$, where $v = \text{const.}$) Thus, the normalized leading-order approximation is an ideal-fluid steady state, and some functional relation between ω_0 and Φ_0 must hold.

Grouping next the terms with the factor ν yields the following equation for the first-order corrections in (4.1a) and (4.1b):

$$(A_1L^2)\,[J(\omega_0, \Phi_0) + J(\omega_0, \Phi_1)] = -\left(\frac{A_0'}{A_0}L^2\right)\omega_0 + (L'L)\left[\xi\frac{\partial\omega_0}{\partial\xi} + \eta\frac{\partial\omega_0}{\partial\eta}\right] + \Delta\omega_0, \tag{4.6}$$

where Δ is the Laplacian in ξ and η, and the prime designates differentiation with respect to τ. Because $\Delta\omega_0$ in (4.6) is independent of τ, the coefficients in the parentheses must be constant. Constancy of $A_0'L^2/A_0$ and $L'L$ leads us to the relationships equivalent to (2.11) and (2.12):

$$L = L(0)\sqrt{1 + \Lambda\tau}, \quad \ln\frac{A_0}{A_0(0)} = \mu\ln\frac{L}{L(0)}, \tag{4.7}$$

where Λ and μ are constants. The smallness of the first-order terms in (4.1a) and (4.1b) guarantees the like behaviour of ζ_M and A_0. Thus, based on our simulations (figure 3), we can conclude that, at least in terms of L and A_0, the criteria of leading-order self-similarity are fulfilled.

The as yet unutilized condition $A_1L^2 = \text{const.}$ carries important information on $\langle J\rangle$. As A_0L^2 is the amplitude of the zero-order co-moving streamfunction, this condition determines the A_1 to A_0 ratio:

$$\frac{A_1}{A_0} = \frac{c}{\max\,\Psi_0} = \frac{c}{\Psi_M} + O(\nu), \quad c = \text{const.}, \quad \Psi_M = \max_{x,y}\Psi, \tag{4.8}$$

where Ψ_M, the local maximum of Ψ assumed within the separatrix, is understood as a function of τ. Equations (4.4) and (4.8) allow rewriting of (4.1) as

$$\zeta = A_0\left[\omega_0(\xi,\eta)+\frac{A_1}{A_0}\nu\omega_1(\xi,\eta)\right]+O(\nu^2)=A_0\left[\omega_0+\frac{c}{\Psi_M}\nu\omega_1\right]+O(\nu^2), \quad (4.9a)$$

$$\psi = A_0L^2\left[\Phi_0+\frac{A_1}{A_0}\nu\Phi_1\right]+O(\nu^2)=A_0L^2\left[\Phi_0+\frac{c}{\Psi_M}\nu\Phi_1\right]+O(\nu^2). \quad (4.9b)$$

Due to (4.9), the Jacobian $J_{x,y}(\zeta,\Psi)$ becomes

$$J_{x,y}(\zeta,\Psi)=\nu A_0^2\frac{c}{\Psi_M}[J_{\xi,\eta}(\omega_1,\Phi_0)+J_{\xi,\eta}(\omega_0,\Phi_1)]+O(\nu^2). \quad (4.10)$$

The right-hand side of (4.10) characterizes the deviation from ideality, i.e. the error in (2.6). To estimate the relative error $\langle J\rangle$ in (2.6), we substitute in (3.1) relationship (4.10) and the two obvious relationships:

$$\frac{\partial\zeta}{\partial x}\frac{\partial\Psi}{\partial y}=A_0^2\frac{\partial\omega_0(\xi,\eta)}{\partial\xi}\frac{\partial\Phi_0(\xi,\eta)}{\partial\eta}+O(\nu), \quad (4.11a)$$

$$\frac{\partial\Psi}{\partial x}\frac{\partial\zeta}{\partial y}=A_0^2\frac{\partial\Phi_0(\xi,\eta)}{\partial\xi}\frac{\partial\omega_0(\xi,\eta)}{\partial\eta}+O(\nu). \quad (4.11b)$$

This yields

$$\langle J\rangle=\frac{\nu C}{\Psi_M}+O(\nu^2), \quad C=\text{const.}, \quad (4.12)$$

which can also be written as

$$\langle J\rangle\Psi_M=\nu C+O(\nu^2). \quad (4.13)$$

Thus, if the quasi-asymptotic state possesses the highest possible degree of self-similarity, then according to (4.13), $\langle J\rangle\Psi_M$ must effectively stabilize at a certain constant level νC. On the other hand, the streamfunction maximum in this process can only decrease; therefore, $\langle J\rangle$ must grow monotonically. So, the important conclusion derived is that, over the viscous time scale, a secular deviation from ideality occurs. All these agree well with the observed behaviour of $\langle J\rangle$ and $\langle J\rangle\Psi_M$ (figure 5). Note that the constant C is independent of the initial condition: according to our computations (using a very long run out to $\tau=20$), this constant can be estimated as $C\approx 3.2$.

5. Elliptical solution as the limiting dipole

The zero-order terms in (4.1) are supposed to represent the scaled decaying dipole as $\nu\to 0$, i.e. the inviscid solution selected by viscosity. Now we are prepared to estimate the zero-order fields based on the computational data. The results of this operation will provide one more test of the validity of our asymptotic theory.

Consider a simulation initialized with a specific dipole and define the normalized fields ω and Φ as $\omega=\zeta/\zeta_M$ and $\Phi=\Psi/\Psi_M$, understanding them as functions of τ, ξ and η. (Clearly, scaling of the vorticity and co-moving streamfunction fields with ζ_M and Ψ_M instead of A_0 and A_0L^2, respectively, does not change the relations (4.12) and (4.13).) Let $\tau_1\neq\tau_2$ be two moments at which the dipole can be regarded as being in the quasi-asymptotic state, i.e. in which $\langle J\rangle\Psi_M$ is practically constant. Considering (4.9*a*) at $\tau=\tau_1$ and $\tau=\tau_2$, we obtain two linear algebraic equations in ω_0 and ω_1

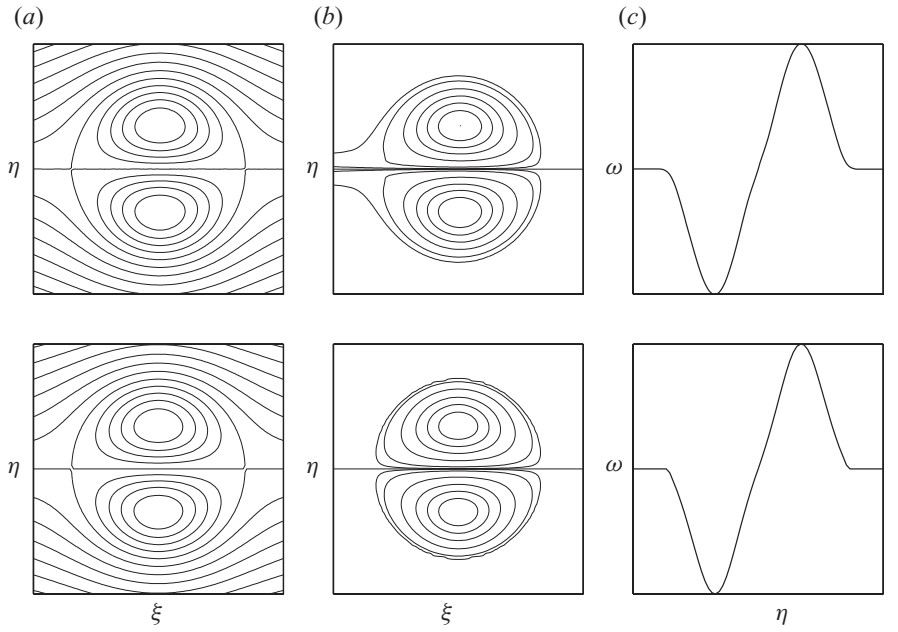

FIGURE 6. The estimated limiting dipole selected by viscosity. Upper row, the leading-order dipole extracted from the simulations ran at $\nu = 0.002$ with spacing 0.1; lower row, the elliptical dipole with $\epsilon = 1.037$.

which imply

$$\omega_0(\xi, \eta) = \frac{\Psi_M(\tau_1)\omega(\tau_1, \xi, \eta) - \Psi_M(\tau_2)\omega(\tau_2, \xi, \eta)}{\Psi_M(\tau_1) - \Psi_M(\tau_2)} + O(\nu^2). \tag{5.1}$$

In the same way Φ_0 is determined from (4.9*b*):

$$\Phi_0(\xi, \eta) = \frac{\Psi_M(\tau_1)\Phi(\tau_1, \xi, \eta) - \Psi_M(\tau_2)\Phi(\tau_2, \xi, \eta)}{\Psi_M(\tau_1) - \Psi_M(\tau_2)} + O(\nu^2). \tag{5.2}$$

We note that the errors in (5.1) and (5.2) are of order ν^2, therefore, at $\nu = 0.002$, these formulas are expected to provide quite a good approximation to the ideal-fluid dipole solution selected by viscosity as $\nu \to 0$. Accordingly, in the scatter-plot of ω_0 versus Φ_0 estimated in this manner, the point scatter must be evidently less than in the scatter plot in figure 4 (see also (4.13)).

The results of extracting the fields ω_0 and Φ_0 and the corresponding ω_0 versus Φ_0 scatter-plot are provided in figures 6 and 7. The data from the simulation initialized with the Lamb–Chaplygin dipole were employed and $\tau_1 = 1.2$ and $\tau_2 = 2$ taken. However, exactly the same results are obtained with other simulations and differently chosen τ_1 and τ_2. The separatrix of the streamfunction field is now essentially symmetric about the η-axis (figure 6*a*), and the dipole wake (in figure 6*b*) is appreciably thinner than in figure 2(*b*) (the contour representing the trail is only 1 % of $\max \omega$). As is evident from figure 7(*a*, *b*), the point scatter in the ω_0 versus Φ_0 scatter-plot is significantly smaller than in the ω versus Φ plot for $\tau = 2$. The argumentation provided in § 3 suggests that, in the exact zero-order dipole, the vorticity field, though continuous, cannot be smooth at the separatrix. We believe that the apparent small-scale smoothness of the vorticity profile at the dipole border (which can be

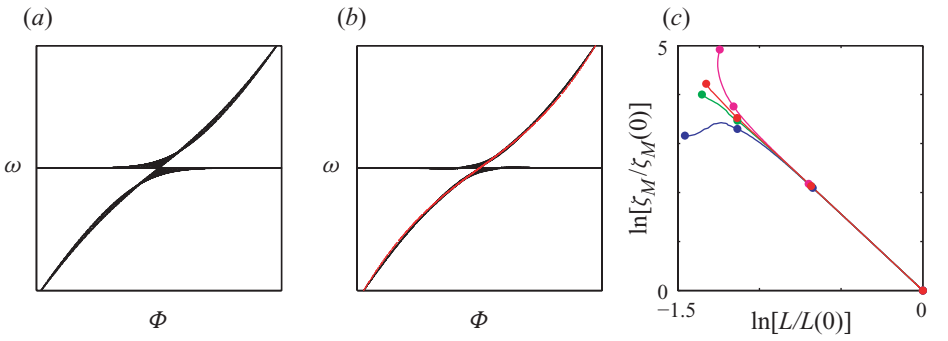

FIGURE 7. The limiting dipole compared to other dipoles. (*a*) Normalized scatter-plot obtained at $\tau = 2$ in the simulations run with $\nu = 0.002$; (*b*) the scatter-plots for the leading-order dipole extracted from the simulations (black) and the ω versus Φ relation for the elliptical dipole with $\epsilon = 1.037$ (red line); (*c*) the $\ln[\zeta_M/\zeta_M(0)]$ versus $\ln[L/L(0)]$ plots for the simulations ran with $\nu = 0.002$ and initialized with the elliptical dipoles with $\epsilon = 0.85$ (blue), $\epsilon = 1$ (green), $\epsilon = 1.037$ (red) and $\epsilon = 1.162$ (pink). Solid circles (from the top left-hand corner to the bottom right-hand corner) indicate the states at $t = 0$, 20, 100 and 500 (i.e. at $\tau = 0$, 0.04, 0.2 and 1). Data used in (*a*) and (*b*) (black scatter-plots) were obtained with spacing 0.1; in (*c*) with 0.05.

recognized in figure 6*c*, in the upper row) is due to the $O(\nu^2)$ errors and grid effects.

The ω_0 versus Φ_0 scatter-plot in figure 7(*b*) resembles that of an elliptical dipole with modest aspect ratio (figure 1*a*). Encouraged by this similarity, we fitted an ellipse to the separatrix of the Φ_0 field and found its aspect ratio to be $\epsilon \approx 1.037$. In figure 6 (lower row), the normalized vorticity and co-moving streamfunction for this elliptic dipole solution are shown, while in figure 7(*b*) the graph of its ω versus Φ dependence (red line) is overlaid upon the scatter-plot for the extracted zero-order fields. Computations initialized with this solution convince us that it is indeed extremely close to the quasi-asymptotic state: from the very beginning, its $\ln[\zeta_M/\zeta_M(0)]$ to $\ln[L/L(0)]$ relation matches almost exactly the asymptotic straight line found in the other simulations (figure 7*c*). The insignificant bending of the red line ($\epsilon = 1.037$) visible in figure 7(*c*) by $\tau = 0.04$ (i.e. by $t = 20$) is a manifestation of the adjustment of the dipole to the grid at the early stage of its evolution.

6. Summary and discussion

The viscous behaviour of a symmetric dipole has been previously considered by several researchers (Juul Rasmussen *et al.* 1996; Nielsen & Juul Rasmussen 1996; van Geffen & van Heijst 1998; Sipp *et al.* 2000), but their numerical simulations were too short to provide the specific shape of the quasi-asymptotic dipole and to finally judge whether the corresponding regime exists. Delbende & Rossi (2009) obtained in their numerical simulations the vorticity profile shown in figure 2, for a specific initial condition, the Lamb–Chaplygin dipole. They also derived a scaling treatment which produces the same leading-order scaling that our analysis predicts; however, the nature of the correction terms in their work differs from that presented above. Also, their characterization of the dependence between the leading-order vorticity and streamfunction by a 'sinh' function is a less exact description than our proposed elliptical dipole. Lastly, the secular breakdown of the ideal scaling profile, which

renders the scaling behaviour only an intermediate time description at a finite ν, went unremarked.

Motivated by previous studies and by our own numerical simulations, we have developed a theory of viscous decay of symmetric two-dimensional dipole vortices. Combining an analytical approach and numerical simulations we showed that, at a fixed viscosity coefficient ν, a dipole cannot adjust in a self-similar state where only the dipole size and strength are affected by viscosity.

The viscosity effect is two-fold. First, viscosity brings any symmetric dipole to a quasi-asymptotic state that (at a given ν) is basically independent of the initial conditions and is close to but different from an ideal-fluid solution, so that some deviation always exists. Then, due to the viscosity, the deviation from this state slowly increases. Thus, one can speak of an intermediate asymptotics.

To explain the observed behaviour, an asymptotic analysis was invoked based on the expansion of the vorticity and streamfunction in asymptotic series with respect to ν, which is in fact the ratio of the advective and viscous time scales. At this stage the hypothesis of separate self-similarity of the zero- and first-order terms was suggested, which relates the evolution of the dipole size and the amplitudes of the leading- and first-order fields to the slow time. This yielded some scaling relations that were verified with the data obtained in numerical simulations.

By employing the approach outlined above we managed to demonstrate that, among the variety of possible shapes given by ideal-fluid dipole solutions, viscosity (at $\nu \to 0$) selects a unique solution. This limiting shape is almost indistinguishable from that of the elliptical dipole solution with the ratio of large to small radii being $\epsilon = 1.037$. The quasi-asymptotic state is, however, fundamentally unsteady: the dipole's size increases, and the amplitude decreases.

The inevitable question that arises from our result is why this specific $\epsilon = 1.037$ quasi-elliptical shape is selected. In two-dimensional flows, energy cascades to large scales and enstrophy to small scales (Kraichnan 1967) where it can be removed by even small viscosity. Therefore, following Leith (1984) one might expect that, among vorticity distributions with the same net energy K, viscosity selects that minimizing enstrophy. More precisely, besides the energy and esnstrophy integrals, there is an infinite set of integrals conserved in two-dimensional inviscid flows. Some of them (like the enstrophy integral) can be strongly dissipated by viscosity, while others (rugged integrals) are less liable to dissipation. We considered the family of elliptical dipole solutions (Kizner & Khvoles 2004; Khvoles *et al.* 2005), the broadest family known to date, confining ourselves to the separatrix aspect ratio $\epsilon \leqslant 1.162$. Once ϵ is fixed, there are only two free parameters that can be varied, the dipole amplitude (or translation speed) and size. In other words, the elliptical dipole solutions can be normalized (i.e. self-similarly deformed) so as to equalize their net energy and, possibly, one more integral characteristic that is supposed to be rugged. As such we considered alternatively the dipole linear momentum P, and $I_m = \iint \zeta^m \,\mathrm{d}x\,\mathrm{d}y$, where $0 \leqslant m < 1$ and the integral is calculated over the area occupied by the positive (cyclonic) vortex. (Note that, for the separatrix aspect ratio $\epsilon \leqslant 1.162$, vorticity ζ in the cyclone is always positive, while at $m = 0$, the integral I_m is the dipole half-area. As for $m = 1$, it is easy to check that it is impossible to normalize the elliptical solutions so as to keep constant both K and I_1, the circulation of the positive vortex.) So, in elliptical solutions normalized in this way, the aspect ratio ϵ can be varied, while keeping K and P or K and I_m constant. Within the normalized elliptical dipoles, we computed the aspect ratio ϵ with minimum net enstrophy. With K and I_m being fixed, the ellipse aspect ratio ϵ_M at which the enstrophy achieves its minimum

value is a monotonic function of m on the interval $0 < m < 0.67$, while ϵ_M lies in the range of $0.98 < \epsilon_M < 1.08$. With fixed K and P, the enstrophy minimum is achieved at $\epsilon_M \approx 1.00$. Thus, there was no indication of some special property associated with $\epsilon = 1.037$.

Under certain circumstances, answers to questions related to the self-organization of two-dimensional and quasi-two-dimensional flows in specific equilibrium states are obtained with statistical mechanics methods, namely, based on the maximum entropy principle (Chavanis, Sommeria & Robert 1996; Bouchet & Sommeria 2002; Chavanis & Sommeria 2002; Holloway 2004). Although this approach is problematic when dealing with essentially continuous vorticity distributions, as a simplifying alternative, vortical pairs composed of patches of uniform vorticity can be considered (such solutions were obtained by Pierrehumbert 1980 and by Dritschel 1995). This might provide a possible path to gain better insight into the dipole selection problem.

This research was supported by Israel Science Foundation grant 628/06. The authors are indebted to M. Cohen for performing some preliminary simulation, and to J. Juul Rasmussen for sharing his code with which this preliminary simulation was performed. Y. Stepanyants and the three anonymous referees are thanked for their helpful comments.

REFERENCES

Bouchet, F. & Sommeria, J. 2002 Emergence of intense jets and Jupiter's Great Red Spot as maximum-entropy structures. *J. Fluid Mech.* **464**, 165–207.

Boyd, J. P. & Ma, H. 1990 Numerical study of elliptical modons using spectral methods. *J. Fluid Mech.* **221**, 597–611.

Chaplygin, S. A. 1903 One case of vortex motion in fluid. *Trans. Phys. Sect. Imperial Mosc. Soc. Friends Nat. Sci.* **11**, 11–14 (translation in *Reg. Chaot. Dyn.* **12** (2007), 102–114).

Chavanis, P. H. & Sommeria, J. 2002 Statistical mechanics of the shallow water systems. *Phys. Rev.* E **65**, 026302.

Chavanis, P. H., Sommeria, J. & Robert, R. 1996 Statistical mechanics of two-dimensional vortices and collisionless stellar systems. *Astrophys. J.* **471**, 385–399.

Delbende, I. & Rossi, M. 2009 The dynamics of a viscous dipole. *Phys. Fluids* **21**, 073605.

Dritschel, D. G. 1995 A general theory for two-dimensional vortex interactions. *J. Fluid Mech.* **293**, 269–303.

van Geffen J. H. J. M. & van Heijst, G. J. F. 1998 Viscous evolution of 2D dipolar vortices. *Fluid Dyn. Res.* **22**, 191–213.

Holloway, G. 2004 From classical to statistical ocean dynamics. *Surv. Geophys.* **25**, 203–219.

Juul Rasmussen, J., Hesthaven, J. S., Lynev, J. P., Nielsen, A. H. & Schmidt, M. R. 1996 Dipolar vortices in two-dimensional flows. *Math. Comput. Simul.* **40**, 207–221.

Kessler, D. A., Koplik, J. & Levine, H. 1988 Pattern selection in fingered growth phenomena. *Adv. Phys.* **37**, 255–339.

Khvoles, R., Berson, D. & Kizner, Z. 2005 The structure and evolution of barotropic elliptical modons. *J. Fluid Mech.* **530**, 1–30.

Kizner, Z., Berson, D. & Khvoles, R. 2002 Baroclinic modon equilibria on the beta-plane: stability and transitions. *J. Fluid Mech.* **468**, 239–270.

Kizner, Z., Berson, D. & Khvoles, R. 2003 Noncircular baroclinic beta-plane modons: constructing stationary solutions. *J. Fluid Mech.* **489**, 199–228.

Kizner, Z. & Khvoles, R. 2004 Two variations on the theme of Lamb–Chaplygin: supersmooth dipole and rotating multipoles. *Reg. Chaot. Dyn.* **9**, 509–518.

Kizner, Z. & Reznik, G. 2010 Localized dipoles: from 2D to rotating shallow water. *Theor. Comput. Fluid Dyn.* **24**, 101–110.

Kraichnan, R. H. 1967 Inertial ranges in two-dimensional turbulence. *Phys. Fluids* **10**, 1417–1423.

Lamb, H. 1895 *Hydrodynamics*, 2nd edn. Cambridge University Press.

Leith, C. E. 1984 Minimum enstrophy vortices. *Phys. Fluids* **27**, 1388–1395.

Meleshko, V. V. & van Heijst, G. J. F. 1994 On Chaplygin's investigations of two-dimensional vortex structures in an inviscid fluid. *J. Fluid Mech.* **272**, 157–182.

Nielsen, A. H. & Juul Rasmussen, J. 1996 Formation and temporal evolution of the Lamb dipole. *Phys. Fluids* **9**, 982–991.

Pierrehumbert, R. T. 1980 A family of steady, translating vortex pairs with distributed vorticity. *J. Fluid Mech.* **99**, 129–144.

Sipp, D., Jacquin, L. & Cossi, C. 2000 Self-adaptation and viscous selection in concentrated two-dimensional vortex dipoles. *Phys. Fluids* **12**, 245–248.

Swaters, G. 1988 Viscous modulation of the Lamb dipole vortex. *Phys. Fluids* **31**, 2745–2747.

Swaters, G. 1991 Dynamical characteristics of decaying Lamb couples. *ZAMP* **42**, 110–121.

Trieling, R., Santbergen, R., van Heijst, G. J. & Kizner, Z. 2010 Barotropic elliptical dipoles on a rotating fluid. *Theor. Comput. Fluid Dyn.* **24**, 111–115.